# Measurement of underlying event properties using charged particles in 13 TeV proton-proton collisions with the ATLAS experiment

Prepared for Czech-Slovak student scientific conference in Physics
May 23-24 Prague, 2016


**Matouš Vozák**

## Abstract

In order to push the high energy frontier of particle physics, the Large Hadron Collider has recently undergone a challenging upgrade to collide protons with two times higher energy than before. New analyses are being carried out by physicists all over the world to measure particles of interests representing building blocks of Standard Model such as W or Higgs bosons, using data at the new collision energy. The environment in which these particles are created tends to be rather busy thanks to all sorts of underlying phenomena. How is this environment, arising from fascinating behavior of proton inner structure, behaving at 13 TeV is a tempting and important study to be performed.

# Contents

# List of Figures

# Chapter 1

# Introduction

Protons are interesting particles to collide mainly for their inner structure. Constituents of protons are quarks and gluons which are in general termed partons because each one of these partons carry part of proton momentum. Therefore, collision of protons at the LHC, where the energy is high enough, can be viewed as interactions between partons inside protons rather than interaction of protons as the whole.

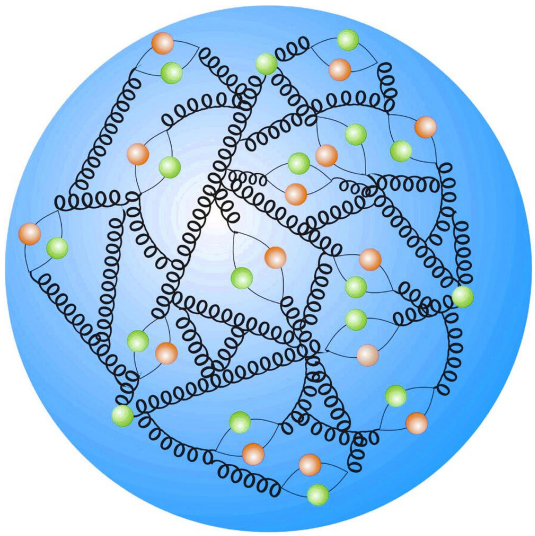

Fig. 1.1: Idea of inner structure of proton. Red balls, green balls and strings representing quarks, antiquarks and gluons respectively [1].

Interaction between partons can be classified as either hard or soft depending on how much momentum was transferred[1]. To create heavy particles such as W or Higgs bosons a lot of momentum has to be transferred. Except for this hard process between pair of partons it is also possible for multiple pairs to interact (multi-parton interaction MPI) with each other giving rise to new particles. As partons carry color charge they can radiate another color charged particles which can further radiate particles and so on to eventually form a cascade. Whether the radiation takes place before or after the collision

[1]When one particle "scatters" off other particle it changes its momentum. The difference between the initial momentum of impacting particle and its momentum after scattering is the momentum transfer. However what is actually measured is not particle momentum but transverse momentum $p_T$ due to geometry layout of the detector. Protons collide with the opposite momentum but the same magnitude $p = p_z$, $p_x = 0 = p_y$, where z-axis is in the direction of the LHC beampipe (anticlockwise), x-axis points toward the center of the LHC ring and y-axis points upwards.

it is termed initial or final state radiation (ISR/FSR). Together with leftover partons from collided proton (beam and beam remnants - BBR) MPI, ISR and FSR represent additional activity, collectively named underlying event (UE), in the collision environment which can negatively contaminate physics measurement.
Unfortunately the UE can not be subtracted from each event. However, it is possible to study its contribution by introducing space regions and several observables sensitive to UE in this regions. Aim of this thesis is to study these observables constructed from primary charged particles. These particles are coming either from collision and have mean life time $\tau_{prim} \geq 0.3 \cdot 10^{-10}$ s or from decays of particles with $\tau \leq \tau_{prim}$.
UE contribution to events can not be calculated as it consists of both hard and soft interaction, where perturbation theory can be applied only for the hard part. Different approach is used in a form of phenomenological models implemented in Monte Carlo generators. These models have several parameters which needs to be tuned to experimental data.

## 1.1 Plane regions

This analysis use the same approach to study UE as in ATLAS studies at center of mass energies 900GeV and 7 TeV [2] by defining $\eta - \phi$ space regions[2]. In each event particle with the highest transverse momentum (leading particle) divide the plane perpendicular to the beampipe by difference in azimuthal angle $|\Delta\phi|$ of particle from leading particle into 3 main regions.

- Toward region $|\Delta\phi| < \pi/3$
- Transverse region $\pi/3 < |\Delta\phi| < 2\pi/3$
- Away region $2\pi/3 < |\Delta\phi|$

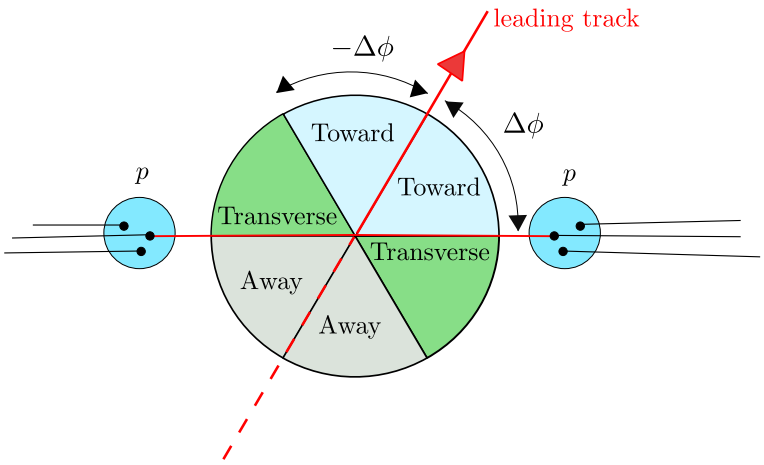


Fig. 1.2: Introduction of toward, transverse and away regions defined using leading track and its difference in azimuthal angle compared to other tracks $\Delta\phi$.

As can be seen from the Fig 1.2 by definition the toward and away regions are contributed from the hardest scattering event leaving the transverse region occupied mainly by UE. Both transverse regions can be also studied separately. As suggested in [7] one of the transverse region could be more active (transverse max) in the case of three jet situation and contain MPI with FSR whereas the other (transverse min) mainly MPI. Subtraction of these two transverse region (transverse diff) could provide information about activity solely from radiation.

[2] Another UE studies were performed for example by CMS at 7 TeV [3], CMS at 13 TeV [4] and CDF at 1.8 TeV [5] and 1.96 TeV [6].

## 1.2 Observables

All measured observables on particle and detector levels are in Tab. 1.1. On detector level these observables are constructed from selected tracks[3](more about selection in section 2). Charged particle density is defined as number of charged particles in a given region divided by $\eta\phi$ area. The same applies for sum of $p_T$ of all particles in the region. These two observables are plotted with respect to the transverse momentum of the leading particle $p_T^{lead}$ and also with respect to the difference in azimuthal angles $|\Delta\phi|$. Last observable is mean particle transverse momentum which is constructed on event-by-event basis and plotted against number of particles $N_{ch}$ and also $p_T^{lead}$.

| | $\langle d^2 N_{ch}/\, d\eta\, d\phi\rangle$ | $\langle d^2 \Sigma p_T/\, d\eta\, d\phi\rangle$ | $\langle mean p_T\rangle$ |
|---|---|---|---|
| Particle level | Mean number of stable charged particles per unit $\eta\phi$ | Mean scalar $p_T$ sum of stable charged particles per unit $\eta\phi$ | average $p_T$ of stable charges particles |
| Detector level | Mean number of selected tracks per unit $\eta\phi$ | Mean scalar $p_T$ sum of selected tracks per unit $\eta\phi$ | average $p_T$ of selected tracks |

Tab. 1.1: Observables on detector and particle level.

[3]As particle flies through detector, it leaves its track - signals in layers of detector- and from these signals is the path of the particle reconstructed. Therefore, particle on detector level is reffered as track.

# Chapter 2

# Selection

The experimental data from the LHC at 13 TeV with integrated luminosity 169 $\mu b^{-1}$ taken in june 2015 were used in this analysis. In particular run 267358 and 267359 with mean number of interactions per bunch crossing $\mu$ 0.003 and 0.007 respectively.
Requirement on passing event and track selection was necessary to reduce background from pile up, cosmic radiation and others.

1. Event selection

   - Good run list applied (pass of events with good luminosity)
   - Hit on either side of Minimum bias trigger scintillator MBTS (called , technically L1_MBTS_1) to fire L1 trigger, this trigger is passed through the LHT and the event is always recorded
   - Presence of a primary vertex
   - Not contain a second vertex with four or more tracks (in order to remove events with more than one interaction per beam crossing)
   - at least one good track in the event with a $p_T > 1\,\text{GeV}$ ( To take events with sufficient hard scattering )

2. Track selection

   - $p_T > 500\,\text{MeV}$ and $|\eta| < 2.5$ .
   - At least 1 pixel hit.
   - If a hit is expected in the innermost pixel layer (IBL), then one is required. The active area coverage of the IBL layer is more than 99%. If a track passes through an inactive IBL module, then a hit is required in the next layer if one is expected. This requirement suppresses tracks from secondaries.
   - At least 6 SCT hits for tracks with a transverse momentum above 500 MeV and $|\eta| < 2.5$. If a track passes through an inactive layer, it is counted as a hit. This makes the selection less sensitive to differences in the number of dead module in data and simulation.
   - The transverse impact parameter $d_0$ calculated with respect to the LHC beam line is required to be less than 1.5mm ($|d_0| < 1.5\,\text{mm}$).
   - The longitudinal impact parameter $z_0$ is calculated with respect to the primary vertex. It is required that the distance between the primary vertex and the track at the point where $d_0$ is measured multiplied by $\sin(\theta)$ is $|z_0|\sin(\theta) < 1.5\,\text{mm}$.
   - If the track $p_T$ exceeds 10 GeV, then the track $\chi^2$ probability must be bigger than 0.01 to suppress mismeasured tracks.

| | Simulation **Events** | % passing | Data **Events** | % passing |
|---|---|---|---|---|
| Before cuts | 10000000 | | 10855221 | |
| After primary vertex and pile up suppression | 9946358 | 99.46% | 9318369 | 85.84% |
| After requiring 1 track above $p_T > 500$ MeV | 9543913 | 95.43% | 8872172 | 81.73% |
| After requiring 1 track above $p_T > 1$ GeV | 7024171 | 70.24% | 6608940 | 60.88 % |
| After requiring 1 track above $p_T > 3$ GeV | 1632579 | 16.32% | 1272989 | 11.72% |
| After requiring 1 track above $p_T > 5$ GeV | 351123 | 3.51% | 244457 | 2.25% |
| After requiring 1 track above $p_T > 10$ GeV | 29023 | 0.29% | 18368 | 0.16% |

Tab. 2.1: Number of events in data and simulation (Pythia A2) before and after applying all the event selection criteria. For data the first row displays the data after GRL and trigger requirement which is not applicable to MC which has first row without any cuts.

| | Simulation **Tracks** | % passing | Data **Tracks** | % passing |
|---|---|---|---|---|
| All Tracks | 383347948 | | 378296616 | |
| $p_T > 500$ MeV | 176287238 | 45.98% | 155797605 | 44.86% |
| $\lvert\eta\rvert < 2.5$ | 172502488 | 44.99% | 152587337 | 43.93% |
| Innermost hit requirement | 160072434 | 41.75% | 141259906 | 40.67% |
| Pixel Hit $> 1$ | 138319599 | 36.08% | 121493317 | 34.98% |
| SCT Hits $> 6$ | 127912396 | 33.36% | 112093875 | 32.27% |
| $\lvert d_0\rvert < 1.5$ mm | 123473650 | 32.20% | 107611208 | 30.98% |
| $z_0 \cdot \sin\theta < 1.5$ mm | 122392824 | 31.92% | 106403246 | 30.63% |
| $\chi^2$ probability | 122392824 | 31.92% | 106403246 | 30.63% |

Tab. 2.2: Number of tracks in data and simulation (Pythia A2) after event selection (without 1 GeV cut) before and after applying all the track selection criteria.

# Chapter 3

# Reconstruction efficiencies

The fact that the detector and other used tools are not 100% effective has to be accounted for. Knowledge of these efficiencies is then used to estimate correction of observables to particle level. Three main sources which effect the results were studied by minimum bias group [9] - trigger, vertex and tracking efficiency.

## 3.1 Trigger efficiency

For this particular analysis Minimum bias trigger scintillator MBTS were used. This trigger is situated on both sides of ATLAS detector and for event to be accounted for the trigger has to fire at least on either sides of MBTS. The trigger efficiency $\epsilon_{trk}$ is taken as the ration of MBTS (full name:EF_noalg_L1_MBTS_1) triggered events to events in control sample (triggered by HLT_mb_sptrk_1). Events selected at L1 are filtered by requirement to have at least two pixel hits with a time over threshold of at least 20 bunch crossings and at least three SCT hits. Additional condition is to reconstruct at least one track with $p_T > 200$ MeV and its longitudinal impact parameter with respect to the center of the ATLAS coordinate system less than 40 mm.
The trigger efficiency parameterized as a function of selected tracks $n_{sel}^{BL}$ is depicted in Fig. 3.1. These selected tracks are different from selected tracks in 2 due to loosen requirement on $z_0^{BL} < 1000$ mm which is applied in order to avoid biasing the vertex position along the beam line[1]. The tigger efficiency is above 98 % and even reaches 100 % for selected tracks $n_{sel}^{BL} > 6$.

## 3.2 Vertex efficiency

Tracks which reconstruct vertex need to pass following criteria

- $p_T > 100$ MeV
- At least 1 Pixel hit
- At least 4 SCT hits
- At least 6 Silicon hits
- Transverse and longitudinal impact parameters as well as their uncertainties calculated with respect to the beam line (BL): $|d_0^{\mathrm{BL}}| < 4\,\mathrm{mm}$, $|z_0^{\mathrm{BL}}| < 1000\,\mathrm{mm}$, $\sigma_{d_0}^{\mathrm{BL}} < 5\,\mathrm{mm}$, and $\sigma_{z_0}^{\mathrm{BL}} < 10\,\mathrm{mm}$

[1]Beam line also referred as beam spot is a mean value of primary vertex (vertex with the highest sum of tracks $p_T$ in an event ) coordinates x,y,z in run.

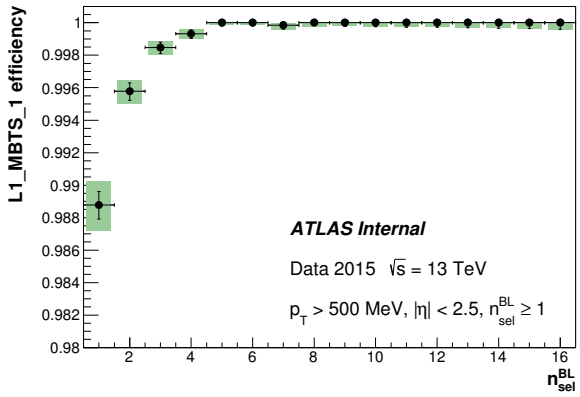


Fig. 3.1: Trigger efficiency plotted as a function of the number of selected tracks $n_{sel}^{BL}$. A reconstructed vertex is not required. The statistical errors are shown as black lines, the total errors as green shaded areas [9].

Vertex efficiency $\epsilon_{vtx}$ is taken as a ratio of MBTS triggered events with reconstructed vertex to all MBTS triggered events after subtraction of non-collision background. Dependence of $\epsilon_{vtx}$ on $\eta$ and $n_{sel}^{BL}$ (with the same definition as for $\epsilon_{trig}$ ) is depicted in Fig. 3.2 where for $\eta$ case it is only for events with $n_{sel}^{BL} = 1$. If the number of selected track $n_{sel}^{BL} > 2$ then the efficiency of vertex reconstruction $\epsilon_{vtx}$ is 100 % . The $p_T^{lead}$ >1 GeV requirement in this analysis shift the $n_{sel}^{BL}$ into higher values Fig. 3.3. Therefore, for most of the events $\epsilon_{trig}$ and $\epsilon_{vtx}$ are equals to 1 and only for small portion of events ( $\approx$ 2 %) are the values different from 1.

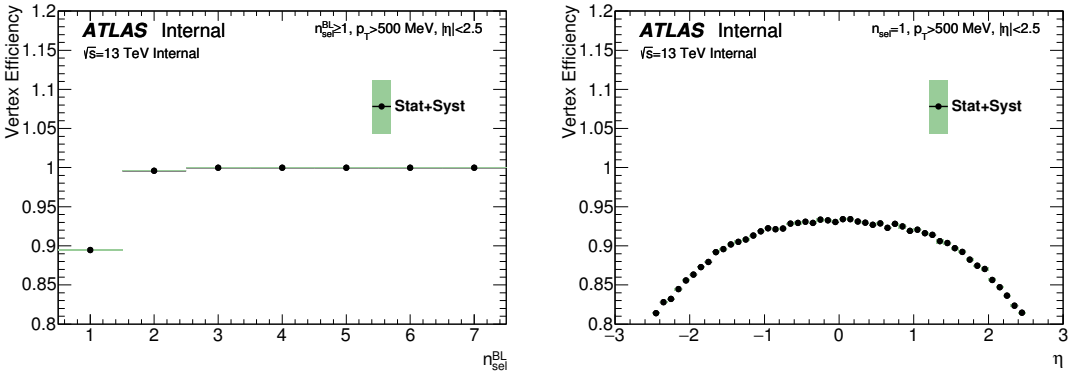


(a) (b)

Fig. 3.2: Vertex efficiency in the data plotted as a function of selected tracks $n_{sel}^{BL}$ **a** and as a function of $\eta$ **b** where the $\epsilon_{vtx}$ is only for $n_{sel}^{BL} = 1$. with respect to the event selection as a function of the number of reconstructed tracks (a) and as function of $\eta$ for exactly one selected track (b). The statistical errors are shown as black lines, the total errors as green shaded areas. The systematic errors are from the subtraction of the non-collision beam background [9].

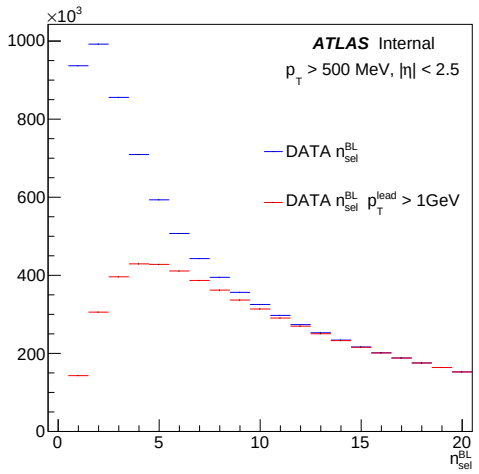


Fig. 3.3: The multiplicity distribution of selected tracks $n_{sel}^{BL}$, with requirement on leading track above $p_T^{lead}$ >1 GeV (**red**) and without (**blue**).

## 3.3 Tracking efficiency

The efficiency to reconstruct a track $\epsilon_{trk}$ is taken from a simulation where truth primary particles are matched to tracks. $\epsilon_{trk}$ is parameterized by $p_T$ and $\eta$ Fig. 3.4. As can be seen from figures tracks are reconstructed with 85 % probability in central rapidity regions. This efficiency decreases towards forward region reaching $\approx$ 67% for $\eta = 2.5$. Dependence of $\epsilon_{trk}$ is rising from $\approx$ 0.875 % at 500 MeV to $\approx$ 0.92% at 100 GeV.

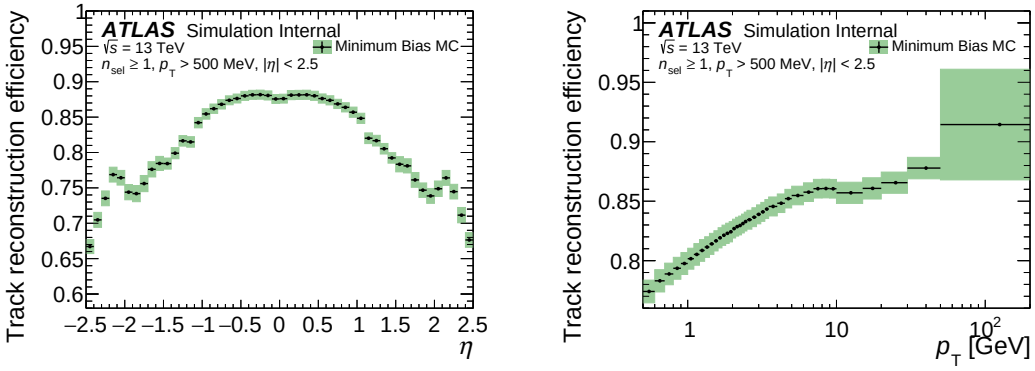


(a) (b)

Fig. 3.4: Tracking efficiency plotted as a function of $\eta$ which is integrated over $p_T$ (**a**) and $p_T$ which is on the other side integrated over $\eta$ (**b**). The total errors as green shaded areas.

### 3.3.1 Fraction of non-primary tracks

The rate of particles which are non-primary is used in determining the final corrections. These particles come from hadronic interaction of particles with material, decay of particles with non-zero strangeness and also from photon conversion. The rate of non-primary particles was obtained by using side-band fits of the MC $d_0$ and $z_0$ distributions to the data. The resulting fraction of non-primaries in data is $0.0228 \pm 0.005$. More information about the procedure in [9].

### 3.3.2 Fraction of strange baryons

Contribution of strange baryons is taken as a background due to their bad reconstruction efficiency and thus is removed. Their modeling is significantly MC generator dependent. EPOS was chosen to estimate this background for its best description of strange baryons in ALICE experiment measurements. Measured fraction of strange baryons

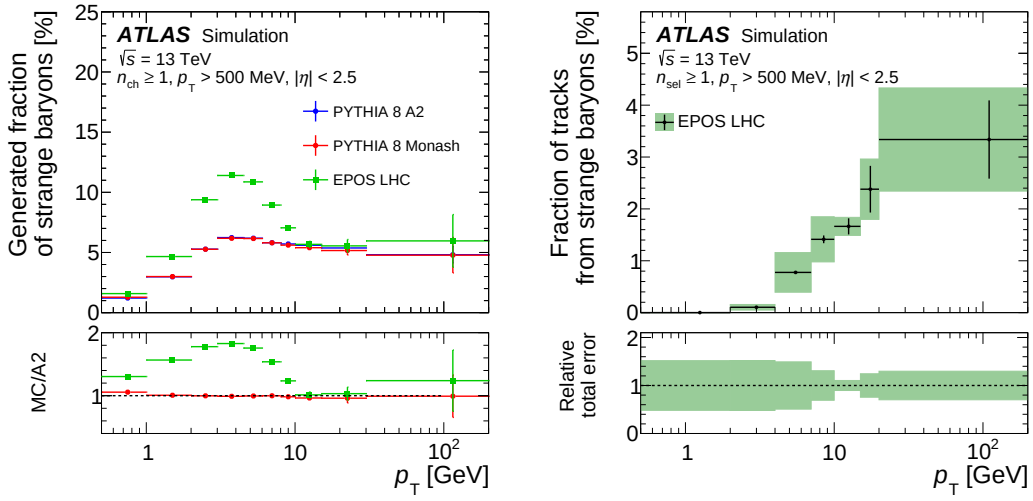


Fig. 3.5: **Left:** Comparison of generated fractions of strange baryons in MC EPOS, Pythia8 A2 and Pythia8 Monash. **Right:** Predicted fraction of tracks due to strange baryons in EPOS generator [9].

# Chapter 4

# Correction

To obtain observables on particle level, they have to be corrected. In this particular analysis two step correction is used. First step is the correction due detector effects. These effects were discussed in previous chapter 3 and include inefficiencies of trigger, vertex and track reconstruction. The observables are multiplied by event and track weights which are constructed from efficiencies in question. The requirement of second correction is due to introduction of regions more or less sensitive to UE. If the leading track is not reconstructed the next track with the highest momentum (subleading) takes its place. However as the subleading track might have different $\phi$ the topology of event is changed and some activity for example in transverse region will contribute to other regions or vice versa. The hit backspace once more (HBOM) method was used to account for this reorientation effect. Application of weights will be discussed at first followed by description of HBOM method.

## 4.1 Event and track weights

Event weight is constructed as one over efficiencies of trigger and vertex reconstruction and is applied on event-by-event basis.

$$w_{ev} = \frac{1}{\epsilon_{trig}(n_{sel}^{BL})} \frac{1}{\epsilon_{vtx}(n_{sel}^{BL}, \eta)} \tag{4.1}$$

The multiplicity of selected tracks with no impact parameter cuts $n_{sel}^{BL}$ is for $p_T^{lead} > 1$GeV high enough (Fig. 3.3 ) making the event weight close to 1 for most of the events. The $\eta$ dependence is taken into consider only for the case with $n_{sel}^{BL} = 1$ hence $\eta$ corresponds to pseudorapidity of leading track.
Track weight as name suggest includes tracking efficiency and also subtraction of fractions with significant contribution.

$$w_{trk} = \frac{1}{\epsilon_{trk}(p_T, \eta)} \cdot (1 - f_{okr}(p_T, \eta) - f_{nonpr}(p_T, \eta) - f_{sb}(p_T)) \tag{4.2}$$

Due to resolution of detector tracks outside the kinematic region ($p_T$, $\eta$) might migrate to it. Fraction of these tracks $f_{okr}$ was estimated using Monte carlo method ( effect of a few %). $f_{nonpr}$ and $f_{sb}$ corresponds to fraction of non-primary particles and fraction of strange baryons respectively which were discussed in 3.3.1 and 3.3.2.
Track weight is applied to discussed observables as follows

- $\Sigma$ $p_T \rightarrow \Sigma_i$ $p_T^i w_{ev} w_{trk}^i$
- $N_{ch} \rightarrow \Sigma_i w_{ev} w_{trk}^i$
- mean $p_T = \Sigma_i$ $p_T^i w_{ev} w_{trk}^i / \Sigma_i w_{ev} w_{trk}^i$

## 4.2 HBOM

Unfortunately applying only track-event weight corrections is not sufficient. To account for other effects such as mentioned reorientation the HBOM method [8] was performed. This method is based on randomly loosing tracks from events according to their track reconstruction efficiency in several iterations. The result is then extrapolation to one step before the 0-th iteration[1]. This method is then performed in each bin for all observables. By default the number of HBOM iteration is 6 + 0-th ( see left Fig. 4.1 ). Each iteration starts with a different seed to avoid correlation between the iterations. In order to avoid tracking efficiency effects between iteration (meaning to keep focus only on correcting reorientation and other effects) additional reweighting of track weight by one over its tracking efficiency is performed in each iteration if the track survives.

The uncertainty of the method is taken as 68 % confidence interval around mean value of generated toy experimental results in -1 (see right Fig. 4.1). For each toy each iteration is smeared according to gaussian distribution with mean as the initial value of observable for given iteration and statistic uncertainty as $\sigma$.

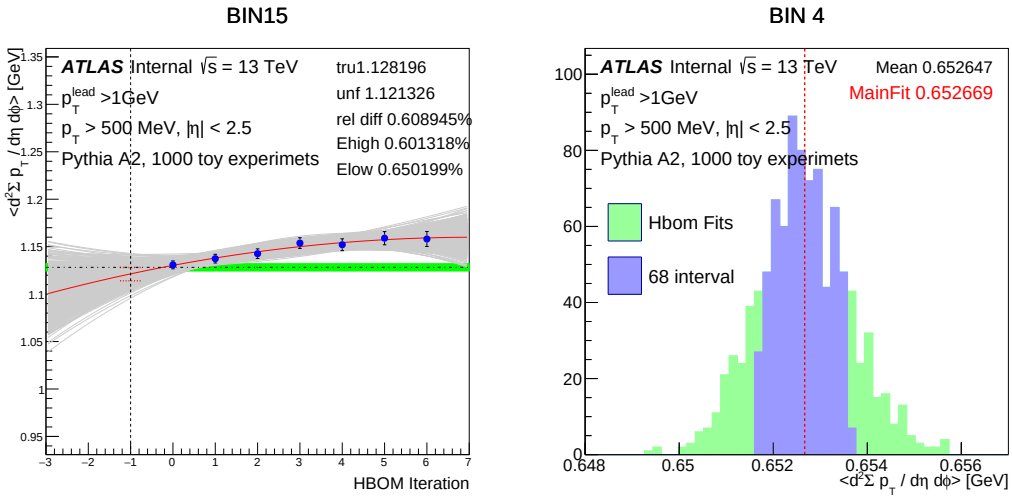


Fig. 4.1: **Left:** Result of extrapolation to -1 using 6 iteration and parameterization by polynomial of second degree in one particular bin for $\Sigma$ $p_T$ wrt $p_T^{lead}$ distribution. Red line represents the main fit, gray lines are 1000 toy experiments fits. For comparison tru distribution is added as dotted horizontal line with green band as statistical uncertainty. **Right:** Distribution of toy experiments values in -1. Red dotted vertical line represents main fit from initial values which is almost the mean of toys in -1.

### 4.2.1 Effect of HBOM correction

To test whether the observables better match particle level with or without HBOM correction, all of them were studied with MC generator Pythia 8 A2. In all following figures for this section there is a comparison between truth level (black line), track-event corrected level (green line) and hbom atop track-event correction (red line). Each figure is also appended by the ratio plot below which is done with respect to the truth level. The following figures is not complete collection of all observables rather just few examples to demonstrate the effect of HBOM correction. For more see upcoming note [11].
All correction on $\Sigma p_T$ and $N_{ch}$ distribution with respect to $p_T^{lead}$ show similar trend Fig. 4.2. The HBOM is not sufficient in first 2-3 bins which is the region with the highest probability to loose tracks.

[1]The 0-th iteration is in this case defined as only track-event weight corrected observables

Non-closure between hbom and truth spectrum in these bins is within 1 % which is still better than closure between track-event corrected and truth spectrum. The rest of the bins are corrected to particle level within the statistic uncertainty except for last bins for some regions where low statistics results in a low quality fit.

The difference between truth track-event corrected spectrum for mean $p_T$ distributions plotted as a

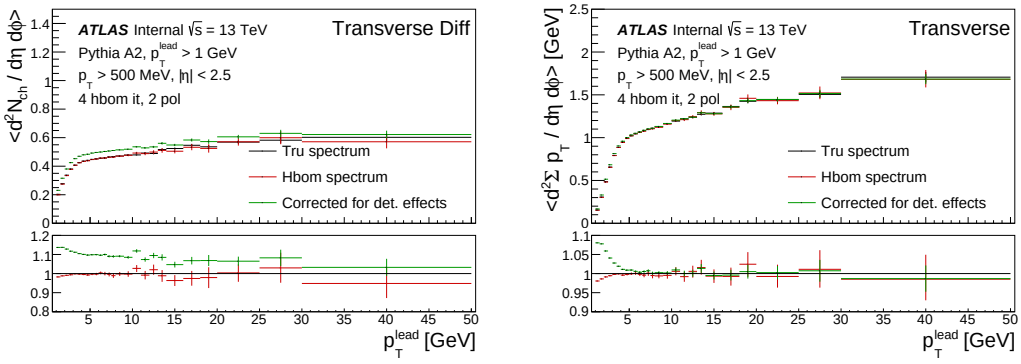


Fig. 4.2: Comparison of truth (black), track-event corrected (green) and hbom (red) spectrums for charged particle density in transverse diff region on the left and sum of $p_T$ in the transverse region on the right both with respect to $p_T^{lead}$.

function of $p_T$ is only within a 3% however the HBOM helps to reduce even this little non-closure 4.3. HBOM also appears to be significant help for mean $p_T$ distribution with respect to $N_{ch}$ where its application bring very good agreement with the truth level except last bins with low statistics. Unfortunately transverse diff region for both mean $p_T$ distributions seems to be troublesome for its high non closure in lots of bins and thus may be eventually taken out of analysis.

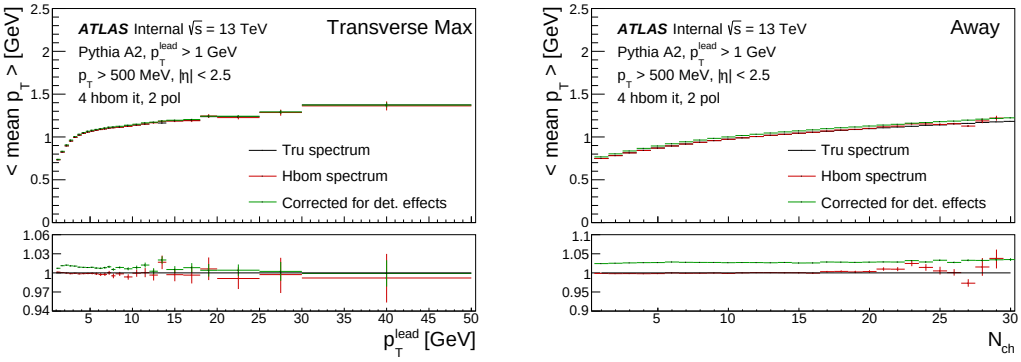


Fig. 4.3: Comparison of truth (black), track-event corrected (green) and hbom (red) spectrums for mean $p_T$ with respect to $p_T^{lead}$ in transverse max region on the left and mean $p_T$ with respect to $N_{ch}$ in the away region on the right.

For distributions $\Sigma p_T$ and $N_{ch}$ plotted as a function of $|\Delta\phi|$ is non-closure between HBOM and truth within 1% . As these two distributions are normalized to number of events taken from distribution of $p_T^{lead}$, HBOM was performed on unnormalized spectrum and also on $p_T^{lead}$ distribution separately and only then were both normalized.

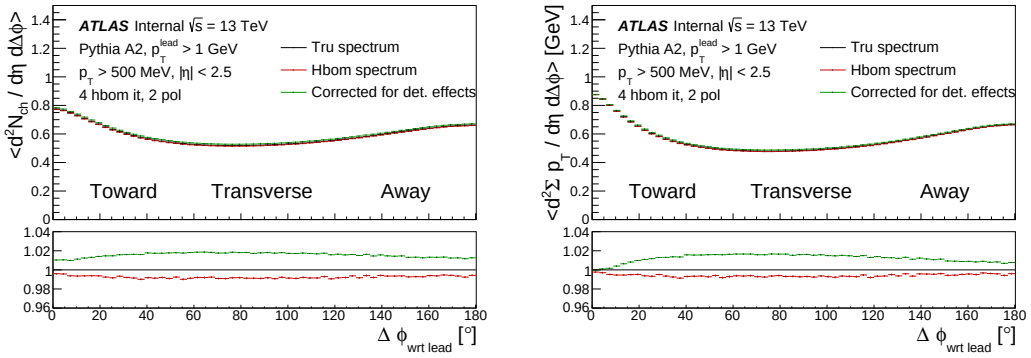


Fig. 4.4: Comparison of truth (black), track-event corrected (green) and hbom (red) spectrums for charged particle density on the left and sum of $p_T$ on the right both with respect to $|\Delta\phi|$.

# Chapter 5

# Uncertainties

HBOM uncertainty ( 68% significance interval ) is applied instead of statistic uncertainty due to their correlation. Several systematic uncertainties are applied as well. Uncertainties from bad material modeling and contribution of non-primary particles are propagated by modification of track weights. As non-closure still persists for some distributions, this difference between truth and hbom level from Pythia 8 A2 is taken as a correction and also as a systematic uncertainty. The choice to use one certain MC is justified by the fact that HBOM method is MC independent. The non-closure correction and uncertainty is applied for distributions plotted as function of $p_T^{lead}$ only in first bins Fig. 4.2 where it reaches maximum of 2% for most of the distributions except in transverse diff region where is the non-closure highest around 20 %. For distributions plotted as a function of $|\Delta\phi|$ is the difference below 0.5 % for all bins. Taken uncertainties for these azimuthal distributions were smoothed. Distributions with respect to $n_{ch}$ have manually setup non-closure band due to existence of few bins without nc correction embodied inside the multiplicity range. Except for transverse diff region where the threshold of mentioned non-closure band was setup on 1 % have all regions default 0.5% as non-closure. Following systematic was also included in these multiplicity bands.

The number of HBOM iteration is by default 6 with parameterization by second polynomial degree. Behavior of all observables with different default setup was studied and will be provided in upcoming note [11]. Some examples are in Fig. 5.1. The difference is significant in the first bins for all $p_T^{lead}$ distributions. The same method as in previous case is applied for distributions plotted as a function of $|\Delta\phi|$.
Example of combination of all used systematic is in Fig. 5.2 and 5.3.

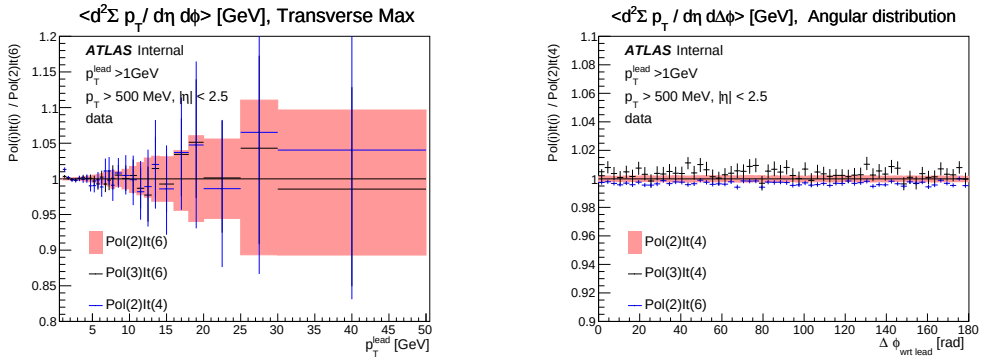


Fig. 5.1: 4 HBOM iteration with 2nd polynomial parametrization and 6 iteration with 3rd polynomial parametrization compared to default 6 iteration and 2nd polynomial parametrization. $\Sigma$ $p_T$ with respect to $p_T^{lead}$ in transverse max on the right and with respect to $|\Delta\phi|$ on the left.

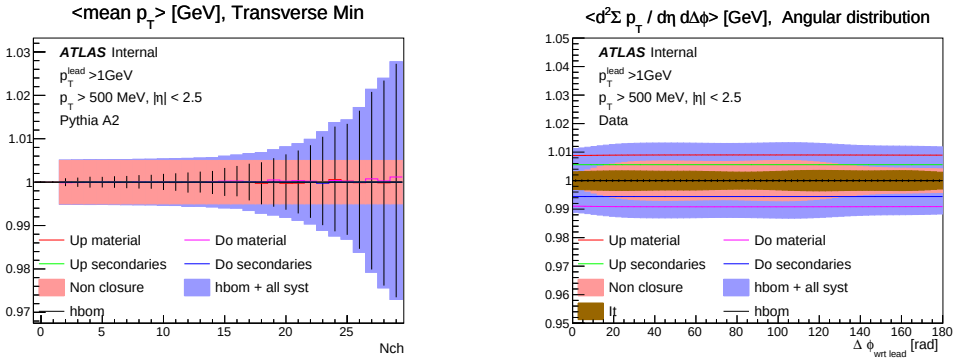


Fig. 5.2: Combination of all used systematic uncertainties for mean $p_T$ plotted as a function of $N_{ch}$ in transverse min region on the left, where the iteration systematic is included in the non-closure band, and $\Sigma$ $p_T$ as a function of $|\Delta\phi|$ on the right.

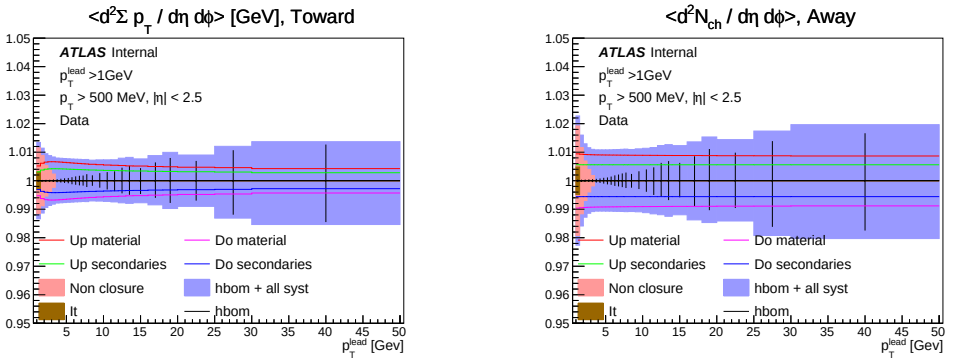


Fig. 5.3: Combination of all used systematic uncertainties for $\Sigma$ $p_T$ in the toward region on the right and $N_{ch}$ in the away region on the left both plotted as functions of $p_T^{lead}$.

# Chapter 6

# Results

The final plots are comparison of several MC generators to HBOM unfolded data. Chosen MCs are Herwig++, Herwig 7, EPOS and from Pythia 8 family A2, Monash and A14. All distributions are normalized to number of events and to $\eta\phi$ space region which means especially for $|\Delta\phi|$ distributions division by a conversion factor $180/2\pi$ to be able compare previous results measured in radians.

## 6.1 $\Sigma$ $p_T$ and $N_{ch}$ distributions wrt $|\Delta\phi|$

In Fig. 6.1 there are $\Sigma$ $p_T$ and $N_{ch}$ distributions plotted as a function of $|\Delta\phi|$ for $p_T^{lead} > 1$, 5, 10 GeV respectively. The toward region, which is defined up to 60 ° has the highest activity for both observables. However the away region is just slightly lower than toward for $p_T^{lead}$ >1 GeV which gives a hint about the topology of events. It seems that events have a pencil like structure. On the other side the transverse region seems to have constant contribution through its whole region.
None of the MCs are describing well the whole toward region neither away for $p_T^{lead}$ >1 GeV. The transverse region is better described with 5% non-closure for A2, EPOS and also A14 for $\Sigma$ $p_T$. As A2 is Minimum bias tune its description for rising $p_T^{lead}$ is worse. However this is not the case for the rest of MCs tuned to describe UE except EPOS.

## 6.2 $N_{ch}$ distribution wrt $p_T^{lead}$

Similar rising trend for charged particle density in all regions for $p_T^{lead} < 5$ GeV can be seen in Fig. 6.2. The rest of the range is however slightly different. Contributions in both toward and away regions are slowly rising with $p_T^{lead}$. Interesting point is that charged particle density is in the away region even higher than in the toward. An explanation was provided in 7 TeV ATLAS analysis [2] . There is less energy to redistribute among other particles in the toward regions as most of it is taken by the leading track. There is a visible plateau called underlying event pedestal In the transverse region from $p_T^{lead} > 5$ GeV meaning that the density of charged particles remains constant even with the harder scattering events. Therefore, the density of underlying event is a constant background with rising $p_T^{lead}$. As mentioned in the introduction the transverse min region contains contribution solely from MPI and this effect is mainly responsible for the UE pedestal which is also visible for charged particle density in this region. On the other hand transverse max is except MPI contributed also from ISR/FSR giving the density distribution slight rise in the region in question.
MCs seems to have failed to describe the data in first bins which is apparently still close to the minimum bias study. But as $p_T^{lead}$ rises the UE tuned MCs start to decrease the non-closure and describe the data reasonably well.

## 6.3 $\Sigma$ $\mathbf{p}_T$ distribution wrt $\mathbf{p}_T^{lead}$

$\Sigma$ $p_T$ distribution is dominant in the toward from all regions due to presence of the leading track followed by the away region Fig. 6.3. Also the transverse region exhibits slow rise in $\Sigma$ $p_T$ whereas the density seemed almost constant.
Non-closure between the data and MCs is similar to the previous case with charged particle density.

## 6.4 Mean $\mathbf{p}_T$ distribution wrt $\mathbf{p}_T^{lead}$

In Fig. 6.4 there are distributions of mean $p_T$ plotted as a function of $p_T^{lead}$ in all regions. Mean $p_T$ is rising in all regions except the transverse min which has a visible pedestal for $\Sigma$ $p_T$ and also for $N_{ch}$. In most of the cases are the data undershooted by MCs but the non-closure is kept within 10 % except for EPOS.

## 6.5 Mean $\mathbf{p}_T$ distribution wrt $\mathbf{N}_{ch}$

Steady rise in mean $p_T$ distribution wrt $N_{ch}$ in all regions can be seen in Fig. 6.5, the only exception is first bins of the toward region due to presence of the leading track.
MCs describe the data within 5% non-closure.

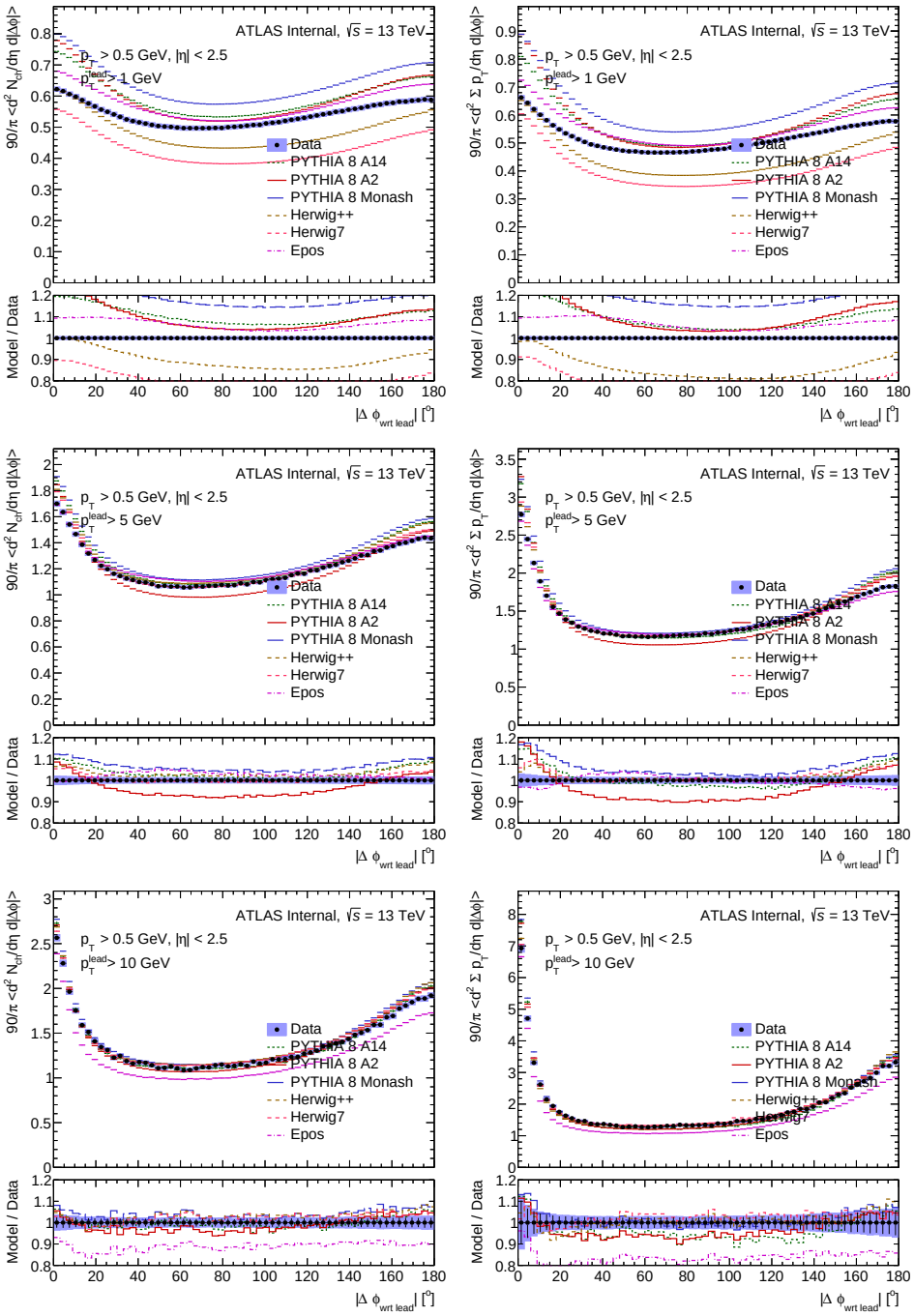


Fig. 6.1: Mean charged particle multiplicity $N_{ch}$ on the left and $\Sigma$ $p_T$ on the right with respect to $|\Delta\phi|$ measured in degrees. Rows of figures are for $p_T^{lead} > 1, 5, 10$ GeV respectively. Blue shaded bands represent combination of statistic and systematic uncertainties given in previous chapters.

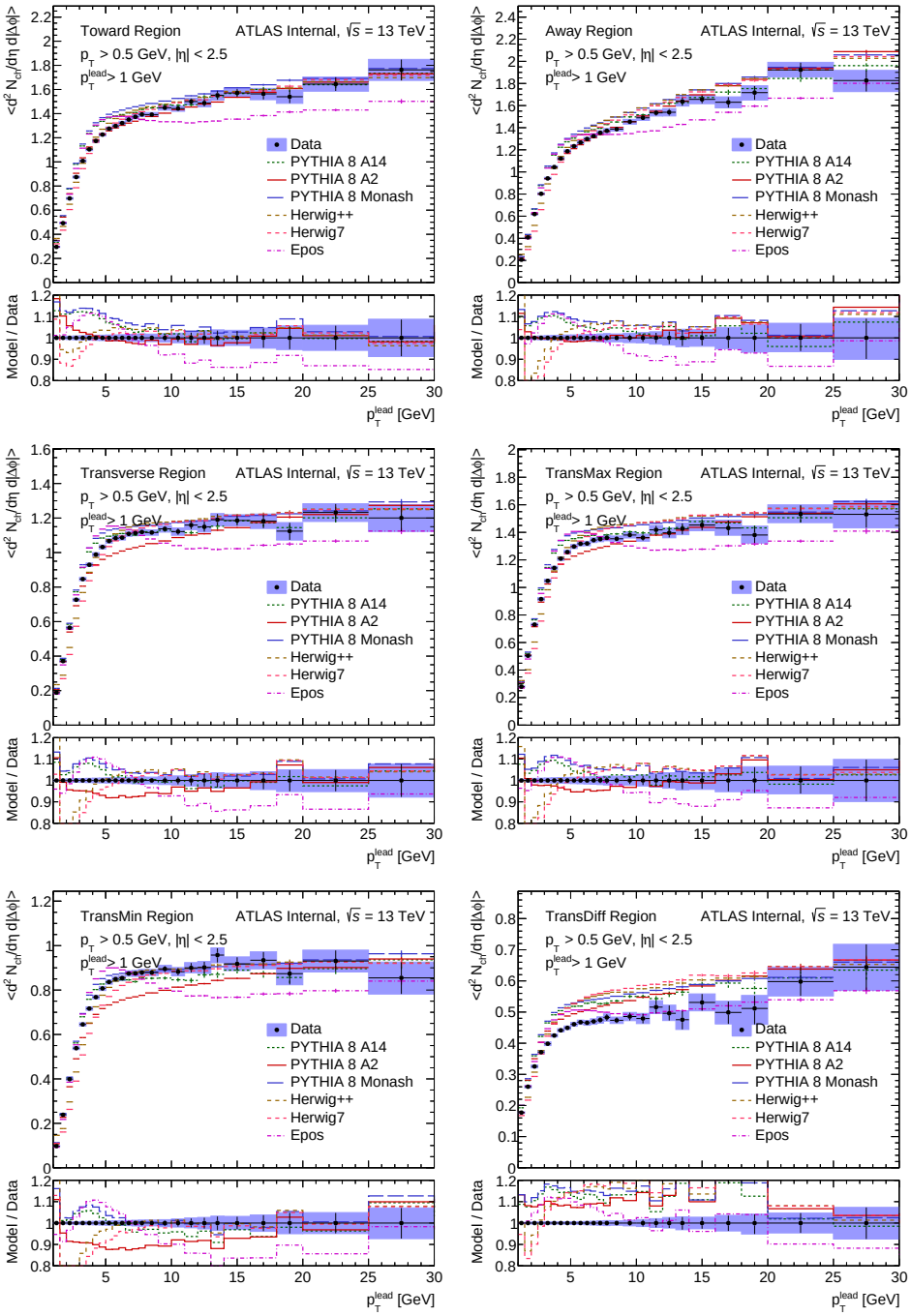


Fig. 6.2: Mean charged particle multiplicity $N_{ch}$ plotted as a function of $p_T^{lead}$ in all studied regions. Blue shaded bands represent combination of statistic and systematic uncertainties given in previous chapters.

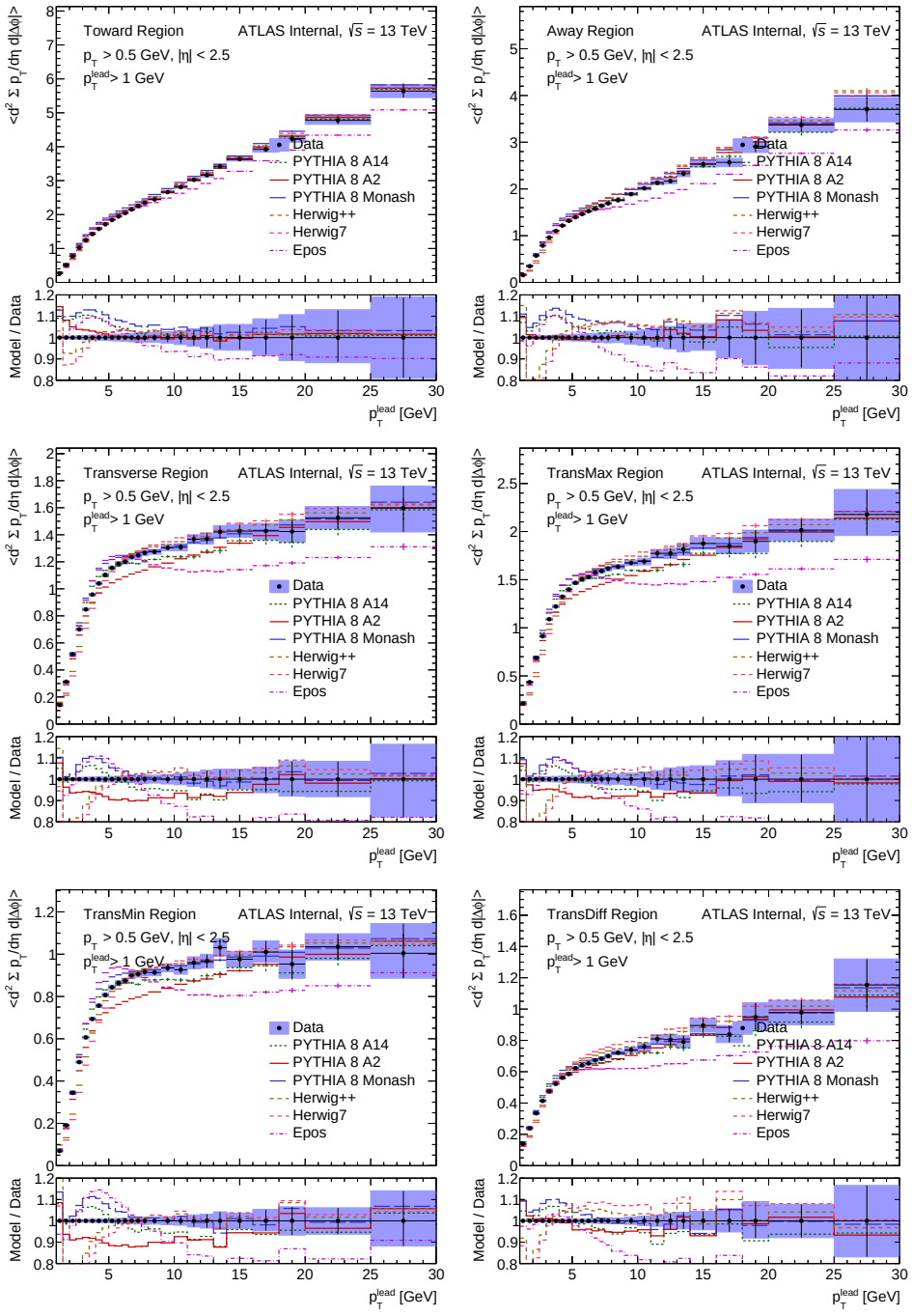


Fig. 6.3: Mean sum of transverse momentum $\Sigma$ $p_T$ plotted as a function of $p_T^{lead}$ in all studied regions. Blue shaded bands represent combination of statistic and systematic uncertainties given in previous chapters.

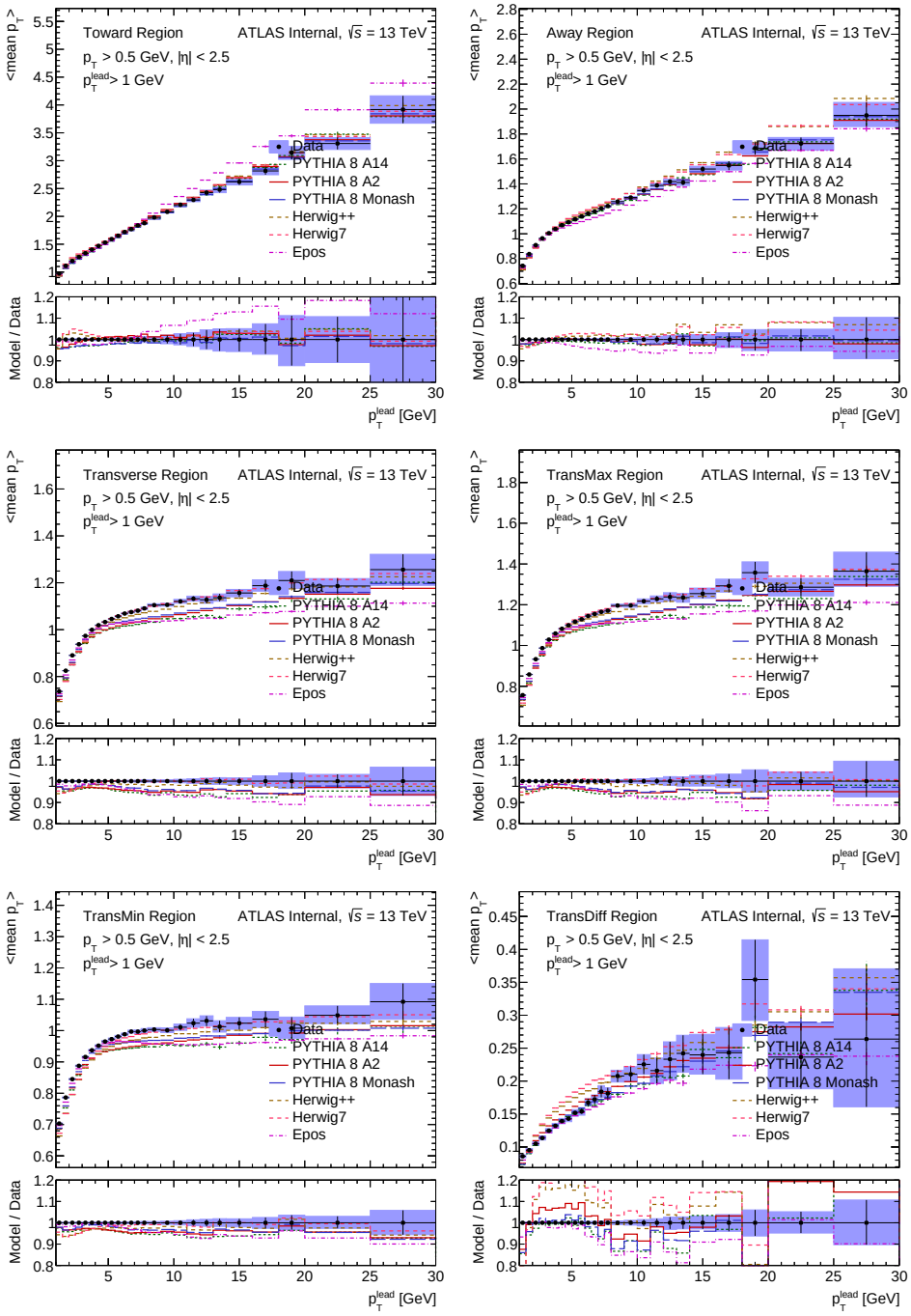


Fig. 6.4: Mean values (normalized for events) of mean of transverse momentum $p_T$ plotted as a function of $p_T^{lead}$ in all studied regions. Blue shaded bands represent combination of statistic and systematic uncertainties given in previous chapters.

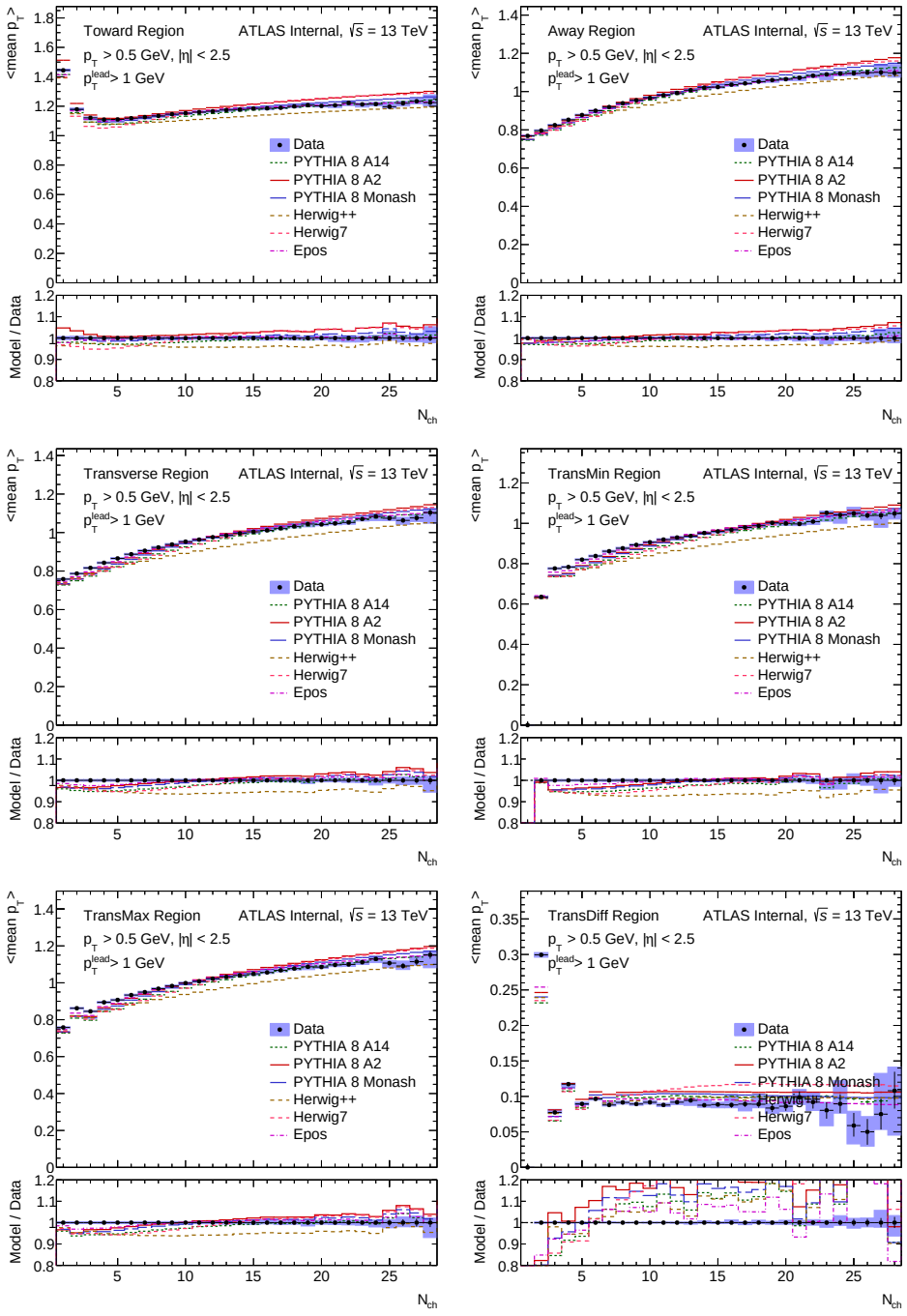


Fig. 6.5: Mean values (normalized for events) of mean of transverse momentum $p_T$ plotted as a function of $N_{ch}$ in all studied regions. Blue shaded bands represent combination of statistic and systematic uncertainties given in previous chapters.

# Chapter 7

# Summary

The behavior of underlying event was studied in 30 distributions sensitive to these effects and constructed from primary charged particles. The approach was similar as in previous analysis by defining few regions in an azimuthal plane perpendicular to the beam pipe using a track with the highest transverse momentum in an event with $p_T$ above 1 GeV. To obtain particle level information, observables were corrected by weights to account for trigger, vertex and track reconstruction efficiency. Additional correction called HBOM were performed as well. This correction helped to improve the non-closure from particle level except few first bins in distributions plotted as a function of $p_T lead$. The data were corrected for this non-closure. As systematic uncertainties were taken material modeling, contribution of secondaries, non-closure and number of HBOM iteration.
The constant behavior (UE plateau) in transverse region with rising $p_T lead$ is observed. Unfortunately the behavior of observables in transverse diff region which was introduced to study initial and final radiation is not stable.
The observables were constructed from the low pile up early data taken by the LHC at 13 TeV and measured with ATLAS. The data were compared with several MC generators namely Herwig++, Herwig7, EPOS, and from Pythia 8 family A2, A14, Monash. The MCs describe the data reasonably well except for low $p_T lead$.
The UE ATLAS measurement at 13 TeV shows rise in activity about 20% in comparison to 7 TeV study [2].
Use of other data samples to improve the statistics in higher $p_T^{lead}$ bins is taken into consideration. However the quality of the new data as pile up or vertex positioning have to analyzed at first. An additional idea is to improve the statistics with leading track trigger HLT_mb_sptrk_pt8_1.

# Bibliography


[1] John Baez, *October diary 2015* http://math.ucr.edu/home/baez/diary/october_2015.html

[2] ATLAS collaboration, *Measurement of underlying event characteristics using charged particles in pp collisions at* $\sqrt{s} = 900$ *GeV and* 7 *TeV with the ATLAS detector*, PhysRevD.83.112001

[3] CMS collaboration, *Measurement of the underlying event in the Drell-Yan process in proton-proton collisions at* $\sqrt{s} = 7$ *TeV*, s10052-012-2080-4

[4] CMS collaboration, *Underlying Event Measurements with Leading Particles and Jets in pp collisions at* $\sqrt{s} = 13$ *TeV*, https://cds.cern.ch/record/2104473

[5] CDF collaboration, *The underlying event in hard interactions at the Tevatron* $\bar{p}p$ *collider*, PhysRevD.70.072002

[6] CDF collaboration, *Studying the Underlying Event in Drell-Yan and High Transverse Momentum Jet Production at the Tevatron*, PhysRevD.82.034001

[7] Marchesini, G. and Webber, B. R., Associated Transverse Energy in Hadronic Jet Production, PhysRevD.38.3419

[8] Monk, James W. and Oropeza-Barrera, *The HBOM Method for Unfolding Detector Effects*,Monk, j.nima.2012.09.045 http://arxiv.org/pdf/1111.4896.pdf

[9] Geraldine and Nurse, Emily and Wozniak, Krzysztof and Martin-Haugh, Stewart and Arnaez, Olivier and Schaefer, Douglas and Kvita, Jiri and Sidebo, Per Edvin and Kuechler, Jan Thomas and Boerner, Daniela and Kepka, Oldrich and Nechansky, Filip and Vozak, Matous and Devesa, Maria Roberta and Iuppa, Roberto and Lysak, Roman and Lukas, Wolfgang and Eckardt, Christoph and Cairo, Valentina and Danninger, Matthias and Cuhadar Donszelmann, Tulay and Chisholm, Andrew and Kulchitsky, Yuri and Plotnikova, Elena and Oide, Hideyuki and Lister, Alison and Pagan Griso, Simone and Gray, Heather and Kar, Deepak and Salzburger, Andreas and Martin, Tim and Tsiareshka, Pavel , *Supporting note for the Minimum Bias publication: Charge particle multiplicity in pp interactions at 13 TeV measured with the ATLAS detector, ATL-COM-PHYS-2015-313*, https://cds.cern.ch/record/2011604

[10] Oldřich Kepka, Deepak Kar, Matouš Vozák, *Leading Track Underlying Event at 13 TeV*, (2015), ATL-COM-PHYS-2015-602, https://cds.cern.ch/record/2030164

[11] Oldřich Kepka, Deepak Kar, Matouš Vozák, Roman Lysak, Andy Buckley, **Upcoming note:***Measurement of charged-particle distributions sensitive to underlying event in* $\sqrt{s} = 13$ *TeV pp collisions with the ATLAS detector at the LHC*